Ab initio molecular dynamics study of the structural and electronic transition in VO_2

Dušan Plašienka* and Roman Martoňák
Department of Experimental Physics, Comenius University in Bratislava, Mlynská Dolina F2, 842 48 Bratislava, Slovakia

Marcus C. Newton
Department of Physics & Astronomy, University of Southampton, Southampton, UK
(Dated: July 20, 2017)

The temperature-induced structural and electronic transformation in VO_2 between the monoclinic M1 and tetragonal rutile phases was studied by means of *ab initio* molecular dynamics, based on density functional theory with Hubbard correction (DFT+U). We compare the structure of both phases, transition temperature and atomic fluctuations both above and below the transition, as well as the phonon density of states and scattering intensity of centroid position, with experimental data. The good quantitative agreement indicates that the chosen DFT+U scheme is able to provide a fairly good description of the energetics of the system. Analysis of the dynamical processes associated with the structural transformation was carried out on the atomic scale by following the time evolution of dimerization amplitudes of vanadium atom chains and the twisting angle of vanadium dimers. The electronic transition was studied by tracing the changes in projected densities of states and their correlation with the evolution of the structural transformation. Our results reveal a strong interconnection between the structural and electronic transformations and show that they take place on the same time scale.

I. INTRODUCTION

Vanadium dioxide VO_2 is a material of long standing interest and is one of the most studied transition metal oxides[1–4]. At 340 K it exhibits a temperature-driven structural transition between low-temperature semiconducting non-magnetic monoclinic phase (M1) and high-temperature metallic paramagnetic tetragonal rutile phase (R)[2,3,5–14]. The transition may be also induced by near-IR or optical photoexcitation[4,14–27]. The M1 phase has an optical gap of 0.6 eV and the insulator-metal transition is accompanied by dramatic change of resistivity spanning over four orders of magnitude. The transition is first order and structurally represents a displacive transition. In both M1 and R phases the V atoms are arranged in 1D chains. While in the R phase all V atoms are equidistant, in the M1 phase they dimerize creating long bonds of length 3.16 Å and short bonds of length 2.62 Å [2] - Fig. 1. The dimerization is accompanied also by zig-zag deformation of chains and doubling of the unit cell in the chain direction. Other phases are also known, most notably another monoclinic phase M2[10,28] where only half of the chain is dimerized. This phase can be stabilized by doping or uniaxial stress but will not be addressed in the present study.

While the transition in VO_2 is obviously of high interest for fundamental reasons, it might potentially be also of practical use in electronic switching and memristive devices as well as in sensing and cloaking materials[29–35]. The theoretical understanding of the transition, however, is still incomplete and represents a puzzle despite a large number of works. The main problem that was extensively studied is the very origin of the insulating properties of the M1 phase. In this respect there are mainly two approaches. The first one interprets the transition within the standard band structure picture as being related to

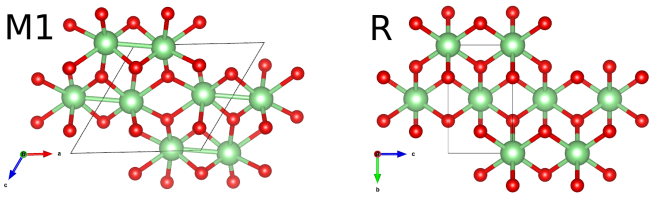

FIG. 1. Structure of M1 and R phases of VO_2[59]. Vanadium atoms are dimerized and octahedra are tilted in the monoclinic structure.

Peierls-type instability of the parent rutile phase. The work by Goodenough[2,36] suggested that the dimerization causes a splitting of the $d_{x^2-y^2}$ band while the zig-zag transversal displacements of V atoms cause a shift of the d_{xz} and d_{yz} bands. Both processes eventually result in creation of the band gap. The other direction attributes the metal-insulator transition upon cooling to strong correlations of d-electrons in V atoms resulting in the Mott insulator[37]. In Ref.[38], employing cluster dynamical mean-field theory in conjunction with DFT, it was concluded that Coulomb correlations are necessary to open the Peierls gap in VO_2. Since the structural and electronic transitions appear to occur at the same time, it raises the "chicken and egg" question which of the two transitions is the primary one. Both these questions and the role of the electronic correlations are still open and actively discussed in the literature[2,4–8,12–18,21–28,31,36–58].

Many studies were devoted to the possibilities of the description of the M1 and R phases by density functional theory (DFT), employing various kinds of approximate functionals. The study in Ref.[46] showed that within the LDA approximation both phases are correctly obtained as local minima of the Kohn-Sham energy. The M1 phase, however, resulted to be semi-metallic rather than insulating. Since both LDA and GGA approximations

are known to underestimate the band gap, in Refs.[9,47,50] the DFT+U approach[60,61] was employed with parameters U=4.2 eV and J=0.8 eV. For static calculations, it was found that this choice provides a satisfactory description of both M1 and R structures as well as a reasonable value of ∼0.6 eV for the band gap. In Ref.[47] it was shown that the introduction of U modifies the imaginary phonons of the R phase in the way which is compatible with the structural transition to the M1 phase.

Considerably less attention was devoted to thermodynamical and dynamical aspects of the transition. Most studies focus on the ideal M1 and R phases at zero temperature and disregard the thermal fluctuations. It is known, however, since long time that the R phase has large value of the Debye-Waller factor which points to strong fluctuations of atomic positions[9,62,63]. A recent study[9] analyzed the phonon density of states in both phases, both experimentally and theoretically and concluded that the rutile phase is stabilized by entropy gain due to phonon softening in the metallic phase.

To our knowledge, so far there was no attempt to directly simulate the phase transition by means of *ab initio* molecular dynamics (MD) and our work attempts to fill this gap in the literature. Our work is meant to test the feasibility of simulating the transition employing a single DFT+U scheme for description of both phases and to provide a detailed picture of the dynamical evolution of atomic and electronic structure across the thermally induced transition.

The paper is organized as follows. In Sec. II, we describe in detail the methods of *ab initio* simulations including choice of the exchange-correlation functional and Hubbard parameters. In Sec. III, we present results that include the evolution of structural and electronic degrees of freedom during the M1-R transition induced by heating, the process of dimerization observed upon cooling, atomic fluctuations in the system at different temperatures and predicted evolution of the scattering intensity observed by coherent X-ray diffraction. We summarize main findings of our work in the Conclusions.

II. METHODS

For the electronic structure calculation we employed the VASP code[64–67] with projector augmented-wave pseudopotentials with six $2s^2 2p^4$ valence electrons for oxygen and five $4s^2 3d^3$ electrons for vanadium. The plane-wave energy cutoff was set to 540 eV and Fermi-Dirac smearing was applied for the electronic states with $\sigma = kT$ appropriately chosen for the actual simulation temperature T.

Ab initio MD simulations were performed in the NPT ensemble using the Parrinello-Rahman barostat[68] and Langevin stochastic thermostat with time step of 2 fs. The simulation samples contained 768 atoms (256 VO_2 units) - Fig. 2 and the supercells were generated as $4 \times 4 \times 4$ unit-cell of M1 and $4 \times 4 \times 8$ unit-cell of R for the two independent heating and cooling simulation protocols, respectively.

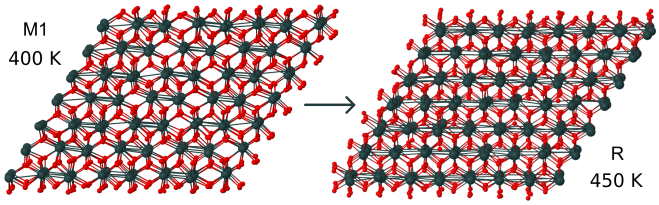

FIG. 2. 768-atomic supercells used in the simulations - M1 before the transition at 400 K and R phase at 450 K.

Electron repulsion in metal $3d$ orbitals may be treated in several ways and properties of VO_2 were therefore in the literature calculated within a wide range of theoretical methods ranging from DFT with Hubbard correction (DFT+U)[9,45,47–50] and hybrid functionals[28,49,69,70] to more sophisticated methods based on dynamical mean-field theory, configuration interaction or quantum Monte Carlo[6,22,38–44,49–52,54–56,71].

In order to describe the electronic structure of the system with both reasonable computational cost and sufficient accuracy we chose to work with the PBE+U functional[60] in Liechtenstein parametrization[61], which appears as a reasonable compromise between the accuracy and computational complexity. Also, we chose to perform non-magnetic calculations within the PBE+U framework since a single DFT- or Hartree-Fock-based methodology that would properly describe both electronic and magnetic properties of both M1 and R phases (as well as monoclinic M2), is not available[49,69,70] as PBE+U scheme incorrectly predicts antiferromagnetic ground state of M1 instead of the experimental nonmagnetic one[47].

Regarding the choice of U and J parameters, we found that the commonly used values U=4.2 eV and J=0.8 eV shift the transition temperature to much higher values and in order to get closer to the experimental conditions it is necessary to modify these two parameters. As noted in Ref.[9], U and J aside from the band gap affect also the energy difference between the M1 and R phases and therefore can be expected to directly influence also the transition temperature observed in simulations. Inspection of the effect of Hubbard parameters on the properties and transition temperature of VO_2 was provided for three different U, J settings, which yield different lattice parameters, M1 band gap and energy difference $\Delta E(T = 0)$ between monoclinic M1 and rutile R phases at $T = 0$. These different settings also resulted in different transition temperatures T_c(U,J) observed in the MD simulations and also in different energy differences $\Delta E(T_c)$ at these temperatures. Results are summarized in Tables I and II. It can be concluded that larger correlation prefers M1 energetically and hence shifts T_c to higher values, in exchange for better band gap estimate.

Hubbard parameters [eV]	PBE (U=J=0)	U = 2.4, J = 0.5	U = 3.15, J = 0.6	U = 4.2, J = 0.8
M1				
a [Å]	5.634	5.660	5.666	5.681
b [Å]	4.560	4.601	4.605	4.607
c [Å]	5.413	5.437	5.443	5.449
β [°]	121.88	122.03	122.04	122.10
M1 band gap [eV]	0.0	0.25	0.36	0.56
R				
a [Å]	4.616	4.626	4.631	4.637
c [Å]	2.773	2.792	2.797	2.799

TABLE I. Lattice parameters of M1 and R and M1 band gap obtained for different U and J parameters.

Hubbard parameters [eV]	PBE (U=J=0)	U = 2.4, J = 0.5	U = 3.15, J = 0.6	U = 4.2, J = 0.8
MD-estimated T_c [K]		300	450	750
ΔE(T_c) [meV/atom]		5	11	15
ΔE($T = 0$) [meV/atom]	-3.7	12.2	21.9	35.0

TABLE II. MD-obtained T_c and energy differences ΔE at $T = 0$ and at $T = T_c$(U,J) for different U and J. Experimental latent heat at $T_c = 340$ K was measured to be 14.7 meV/atom[9].

In our work we have also simulated smaller 96 atomic system with all three U, J settings and the observed T_c were identical to the results coming from 768 atomic system. This suggests that the system size is adequate for proper phonon sampling and observation of the transition.

For our purpose the most suitable values of U and J were found to be U=3.15 eV and J=0.6 eV, which yield the best compromise between the band gap, energetics of VO_2 phases and MD-estimated T_c between M1 and R (450 K). All of the following results described in the next section were calculated with these values and the corresponding band structures of M1 and R phases and their projected electronic densities of states (pDOS) are shown in Figs. 3 and 4, respectively. Our curves of pDOS agree well with similar DFT+U calculations[47,50] as well as with DFT+U+V approach[71] and to a certain degree also to DFT+DMFT calculations[38,44,56].

III. RESULTS

A. M1-R transition - atomic structure

In order to monitor the evolution of the system across the transition we focus on two structural quantities - dimerization amplitudes (DA) of chains of V atoms and the zig-zag displacement (tilt) of V-V dimers. Dimerization amplitude of an individual chain is defined by the formula

$$d = \frac{1}{n}\sum_{j=1}^{n}(-1)^j \Delta x_j, \tag{1}$$

where $j = 1...n$ is the index of a chain atom (with total of $n = 8$ atoms in each chain within the supercell) and Δx_j is the deviation of V atom coordinate along the chain from its ideal position in the R phase. The dimerization amplitude for each i-th chain - d_i hence for the R phase equals zero, while for M1 it is 0.169 Å for an optimized ($T = 0$) structure. There are 32 chains in our simulation sample (each with eight V atoms) whose DA were averaged to obtain the mean order parameter.

The tilting order parameter is defined here as the average angle δ between the vanadium dimers and the $\vec{a}$-axis (in M1 supercell geometry). This so-called twisting angle[8] yields 0 in the R phase and $\approx 7.5°$ in M1 at $T = 0$. There are 128 dimers in our simulation sample and the tilting order parameter was taken as the average twisting angle from all these dimers.

We start with the transition induced by heating the M1 phase. After heating the system from 350 K to 400 K we observed that the system attempts transitions from M1 to R phase which were exhibited by large fluctuations of some DA towards low values - Fig. 5. This shows that some chains were fairly disrupted within certain time intervals during the MD run. This regular loss of the long-range order between some dimers is an indication that the transitions from M1 to R already tries to initiate but within 18 ps of the simulation time the monoclinic phase persisted. It is quite possible that if we could wait a longer time the system could eventually transform from M1 to R. However, such a test would be prohibitively

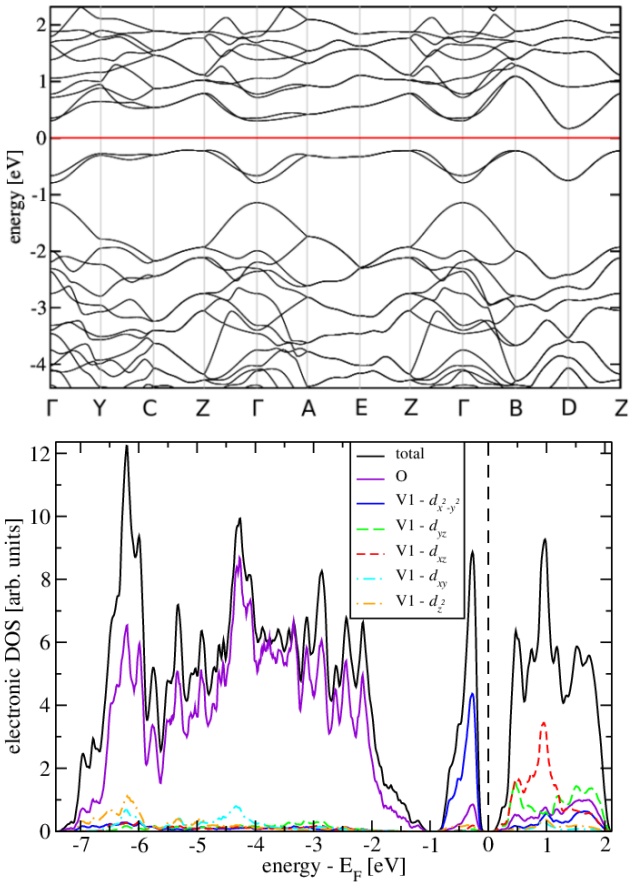

FIG. 3. Band structure along Γ-Y-C-Z-Γ-A-E-Z-Γ-B-D-Z path[2] and pDOS in the local geometry of V1 atoms[2] for optimized M1 phase.

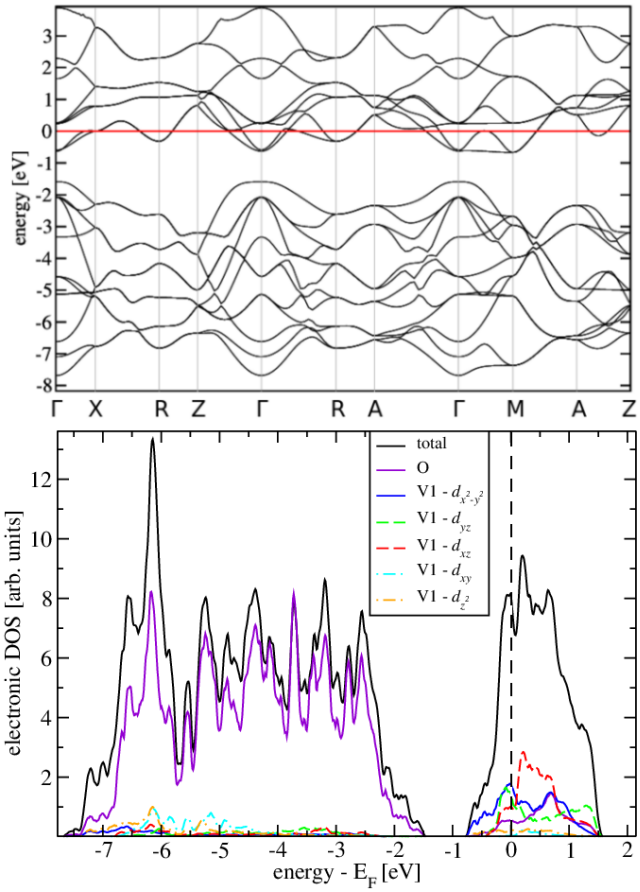

FIG. 4. Band structure along Γ-X-R-Z-Γ-R-A-Γ-M-A-Z path[2] and pDOS in the local geometry of V1 atoms[2] for optimized R phase.

CPU time expensive.

Increasing temperature to 450 K allowed the structural transition from M1 to R to complete within few ps. A video of this process is available within the Supplemental Material. Fig. 6 shows the evolution of DA and twisting angles across the transition. The decrease of DA from ≈ 0.15 Å to 0 proceeds simultaneously with the adaptation of twisting angles from 7° to 0 (see also Ref.[8]). This indicates that there is no separation between dimerization and tilting processes during the transition. After the transition to the R phase, fluctuations of individual DA are considerably larger than in M1, which is directly related to the large fluctuations of V atoms.

Alongside with the evolution of DA and twisting angle, the evolution of the M1-R transformation can be represented by plotting V-V radial distribution functions (RDFs) from several short time intervals during the transformation. In Fig. 7, there are four curves showing V-V RDFs calculated from different time intervals - before the onset of the transition in the M1 phase, during the transition and after it in the R phase. The M1 V-V RDF is characterized by relatively sharp first two peaks that upon transition merge into a broad peak where the presence of two peaks is still visible. This might possibly be due to the excessive tendency of vanadium atoms to dimerize even in the R phase that can be attributed to the the DFT+U scheme employed[53]. Experimentally it was shown in Ref.[72] that no local dimers are present in the R phase.

B. M1-R transition - electronic structure

A standard band structure picture provides a description of M1 band gap as a mutual effect of V-V dimerization, which causes splitting of V-$d_{x^2-y^2}$ states and zig-zag displacement of dimers (tilting) that leads to energetic upshift of V-d_{xz} and d_{yz} states due to the increased V_d-O_p overlap, in the local geometry of V1 atoms[2,12,28,36,38,44,56]. The Peierls-like instability hence, in standard notation, applies to a_{1g} states in an embedded background of e_g^π states.

The time evolution of pDOS during the M1 to R phase transition that occurred in the simulations at 450 K is shown in Fig. 8. We note that within the applied PBE+U scheme the band gap drops to nearly zero value even before the transition because of thermal fluctuations, effec-

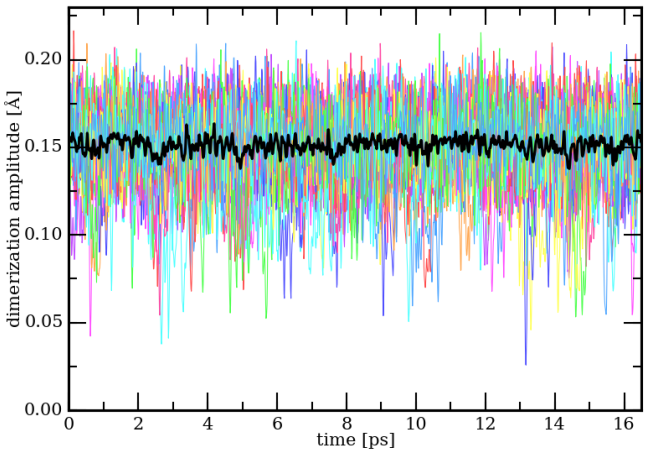

FIG. 5. Evolution of dimerization amplitudes in M1 at 400 K showing large fluctuations of some chain DA in certain time intervals. Black curve represents average of all DA.

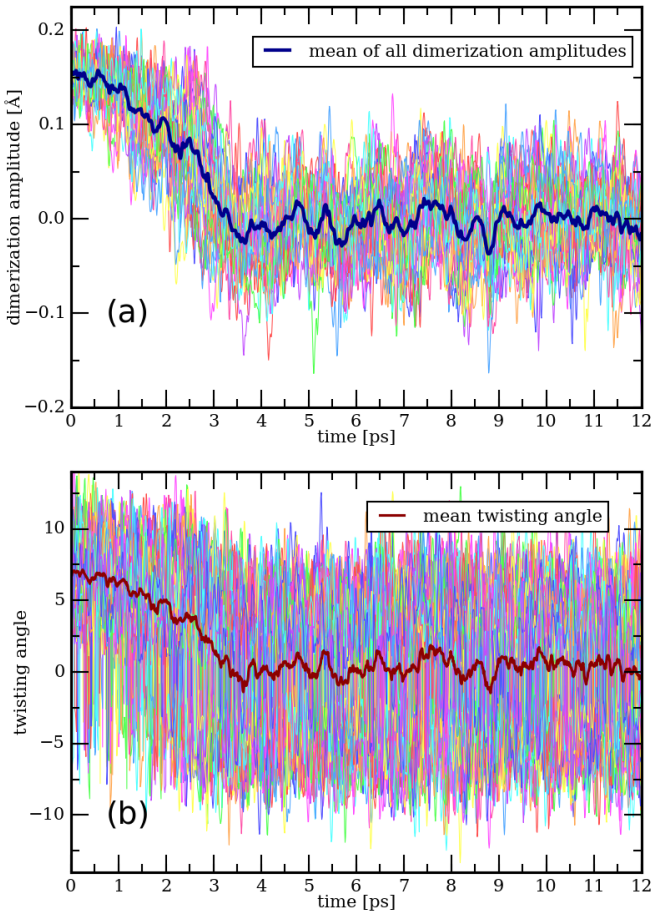

FIG. 6. M1 to R transition at 450 K showing sudden decrease of (a) dimerization amplitudes and of (b) twisting angles. Different colors of curves distinguish between individual chain DA and dimer twisting angles, while blue curve in (a) and red curve in (b) represent mean DA and mean twisting angle, respectively.

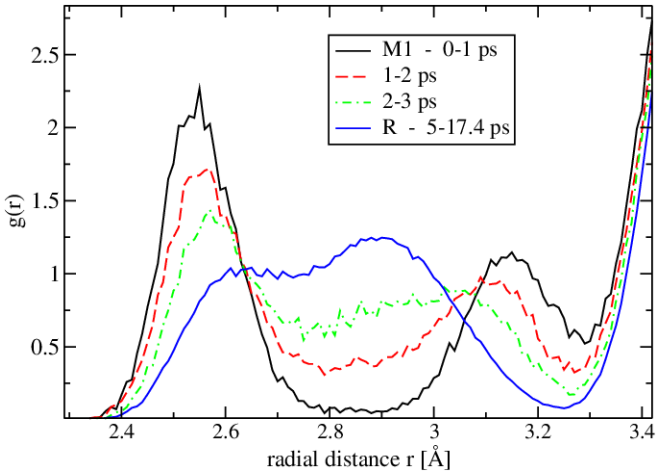

FIG. 7. Evolution of V-V RDF during the transition.

tively turning the M1 phase, semiconducting at $T = 0$, into a semimetal. The principal change in pDOS occurs for a_{1g} states that, after being split in dimerized M1 (0.01 ps), become merged after the transition into R (3.2 ps). At the same time, disappearance of tilting brings energy of e_g^π states below the Fermi level E_F and the states become partially occupied. The V1-d_{z^2} and d_{xy}-derived states, which participate in V-O bonds, do not change much upon the transition.

The correlation between electronic and atomic structure (Fig. 8 and Fig. 6, respectively) indicates that these two aspects of M1-R transformation are closely related and we did not observe any evidence of separation between electronic and structural transition. Also, the two different types of atomic displacements - loss of dimerization and loss of tilting, that are directly reflected in a_1^g anti-splitting and e_g^π energy lowering, respectively, proceed mutually as well, as one could already conclude from Fig. 6.

C. R-M1 transition

After obtaining the R phase, we also tried to decrease the temperature in order to study the symmetry-breaking process in the reverse R to M1 transition. We found that cooling rate (which is adjustable in NPT simulation) crucially influences the final product of the dimerization process. If fast quenching was applied (temperature dropped by 100 K in 2 ps), a dimerized form with randomly distributed V-V dimers was created. On the other hand, if considerably slower cooling rate was applied (decrease by 100 K lasted for over 15 ps), a much more organized state was obtained - Fig. 9. In this state, most of the individual dimerized chains emerged properly, but their overall arrangement was not regular as it is in the M1 phase. The failure of V-V dimers to organize on a long-range scale may be attributed to the limited simulation time that is accessible in our first-principles dynamical

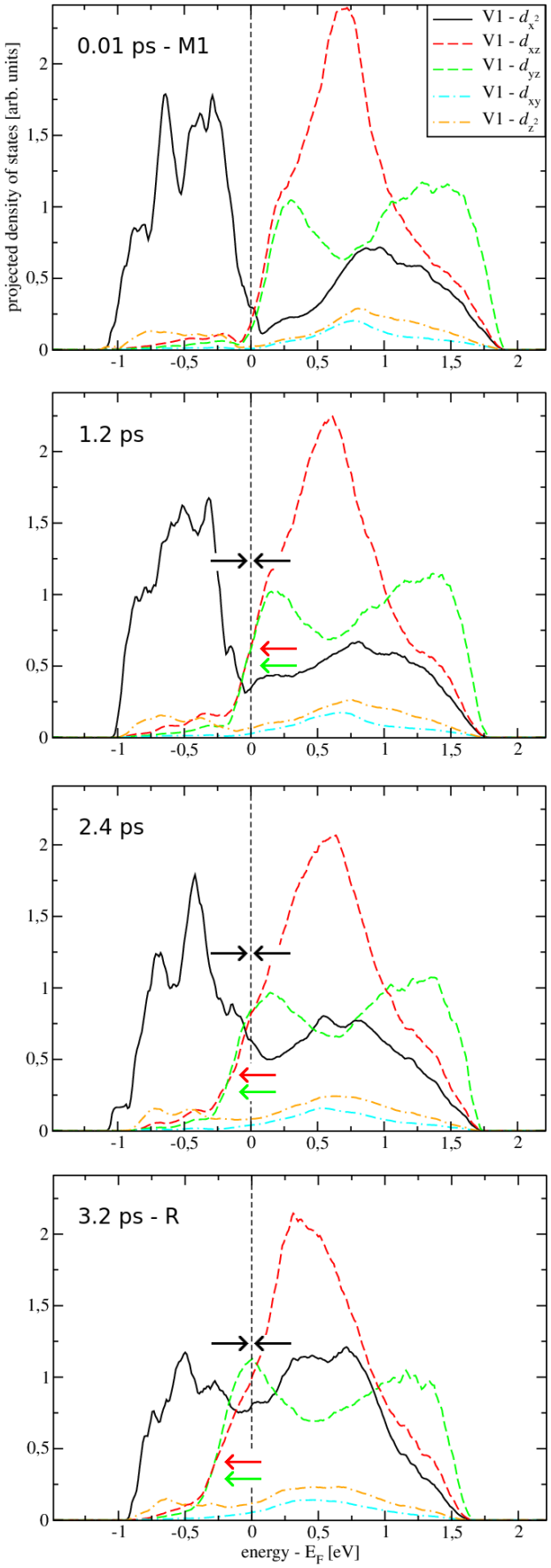

FIG. 8. Evolution of projected densities of states during the transition from initial M1 to final R phase at 450 K depicted at 0.01 ps (M1), 1.2 ps, 2.4 ps and at 3.2 ps (R). Arrows denote principal changes observed for d-projected states.

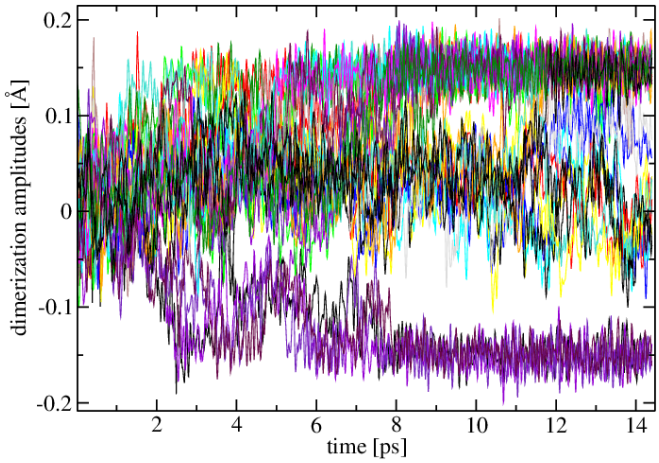

FIG. 9. Evolution of dimerization amplitudes during slow cooling of R phase to 300 K. Various colors differentiate between DA of individual chains.

study. The system upon cooling dimerizes in order to decrease its energy, but follows a randomly chosen pathway on the energy landscape, which usually leads into a metastable local minimum (corresponding to dimerized, but not fully-organized crystalline state). The system afterwards remains trapped in this state and reaching the global minimum requires a longer time scale. This might be partially avoided by using very slow thermal equilibration enabling system to explore a larger region of the configuration space, in analogy to the phenomenon of glass formation via rapid melt quenching, where disordered system is formed from the liquid upon fast quenching, while at lower cooling rates a regular crystal can be obtained instead.

D. Atomic fluctuations in M1 and R phases

The calculated values of static fluctuations of V and O atoms show good agreement with experimental findings - Table III. Fluctuations of lighter O atoms are greater than fluctuations of V atoms in the M1 phase at 300 K by a factor of 1.4, while in the R phase at 450 K the opposite is true and $\langle u \rangle_V^2$ is nearly 1.5 times higher than $\langle u \rangle_O^2$, according to the current simulations.

These large fluctuations of V atoms in the R phase give rise to the large Debye-Waller factors that are observed in XRD experiments[63]. This implies that V atoms remain relatively long time far away from their mean positions in R indicating a more flat energy surface for the displacement of V atomic positions, in contrast to M1, where the motion of V atoms in dimers is more constrained.

fluctuations [Å^2]	experiment - Ref.[73]	simulations - Ref.[9]	current simulations
M1			
	$T = 298$ K		$T = 300$ K
$\langle u^2 \rangle_V$	0.0114		0.0102
$\langle u^2 \rangle_O$	0.0159		0.0142
R			
	$T = 470$ K	$T = 425$ K	$T = 450$ K
$\langle u^2 \rangle_V$	0.036	0.037	0.0348
$\langle u^2 \rangle_O$	0.028	0.021	0.0235

TABLE III. Calculated and experimental values of fluctuations of V and O atoms in M1 and R phases. Current simulations are given in the third column.

E. Phonon density of states

Phonon density of states (PDOS) provides an important information about the vibrational spectrum of the system and can be measured by inelastic neutron scattering. Experimental data for VO_2 for both M1 and R phases are available in Ref.[9]. We computed the PDOS for our system in the M1 phase at $T = 400$ K and in the R phase at $T = 450$ K by calculating Fourier transform of the velocity autocorrelation function averaged over MD trajectory with length about 10 ps in both phases. The results are shown in Fig.10 and can be compared with the experimental data shown in Fig.1 in Ref.[9]. It can be seen that the quantitative agreement between the theoretical and experimental data is quite good for energies below 60 meV while becoming somewhat worse at higher energies. Qualitatively, both data agree well and our MD-calculated PDOS also clearly shows that the phonons in the R phase are softer that in the M1 phase. This is an important observation since phonon softening in the R phase was in Ref.[9] identified as the key ingredient in the stabilization of the R phase at higher temperatures.

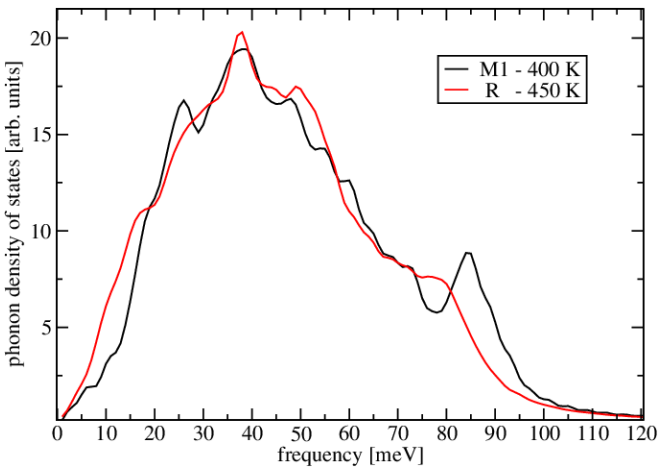

FIG. 10. Normalized phonon density of states in the M1 phase at $T = 400$ K and in the R phase at $T = 450$ K.

F. Coherent X-ray diffraction

It is useful to contrast *ab initio* calculations with complementary ultra-fast pump-probe coherent X-ray diffraction experiments that provide access to femtosecond time-resolution and Ångstrom spatial resolution. Such experiments have become feasible with the recent advent of 4$^{\text{th}}$ generation X-ray free electron laser (XFEL) synchrotron facilities such as the European XFEL. The spatially varying far-field scattering amplitude distribution is proportional to the exponentiated phase associated with scattering from each atom in the supercell. Monitoring changes in the simulated scattering angle and intensity from the speckle pattern provides direct comparison of theory with experiment.

Bragg coherent X-ray diffraction imaging (BCXDI) is a lens-less imaging technique that permits imaging of crystalline materials with a sub-angstrom sensitivity. It is largely non-destructive and provides strain tensor information at the surface and throughout the bulk of a material. Experimentally, BCXDI is routinely performed at 3$^{\text{rd}}$ generation synchrotron facilities by illuminating a sample with a spatially coherent X-ray source while ensuring that the coherence length exceeds the dimensions of the crystal. In the Bragg reflection geometry, scattered light from the crystal interferes in the far-field, producing a three-dimensional k-space speckle pattern. The diffracted intensity is measured using an area X-ray detector which is positioned far enough away from the sample to resolve the finest fringes of the speckle pattern. The third dimension is obtained by rotating the Ewald sphere through the Bragg condition while maintaining a largely fixed incident ($\mathbf{k}_i$) and reflected ($\mathbf{k}_f$) wave vector. Iterative phase reconstruction methods are then used to recover the complex three-dimensional electron density and phase information. The displacement of ions throughout the bulk is directly related to the phase and can be used to obtain strain information according to the relation $\phi = \mathbf{Q} \cdot \mathbf{u}$, where $\mathbf{Q}$ is a particular reciprocal lattice point and $\mathbf{u}$ is the atomic displacement.[74–78]

With the advent of 4$^{\text{th}}$ generation X-ray free electron laser (XFEL) synchrotron facilities, it has become possible to study ultra-fast structural dynamics using femto-

second coherent X-ray pulses. When combined with a femto-second optical excitation source, it is possible to perform stroboscopic measurements in a pump-probe scheme[79].

Direct comparison of ultra-fast pump-probe coherent X-ray diffraction experiments with *ab initio* calculations can be made by simulating coherent X-ray scattering from the supercell for each time frame. This is achieved by defining a static reference lattice at the initial low temperature phase of the system (i.e the M1 phase) that is the average of each atomic position over a predefined time interval (Δt):

$$\mathbf{p}_j = \frac{1}{\Delta t} \sum_{t_0} \mathbf{r}_j(t). \tag{2}$$

For each subsequent time frame, the displacement of each atom from this equilibrium position is then given by:

$$\mathbf{u}_j(t) = \mathbf{r}_j(t) - \mathbf{p}_j. \tag{3}$$

The spatially varying far-field scattering amplitude distribution is proportional to the exponentiated phase associated with scattering from each atom in the supercell:

$$A(\mathbf{q}, t) \propto \sum_j f_j \; e^{-i\mathbf{q}\cdot\mathbf{u}_j(t)}, \tag{4}$$

where $\mathbf{q} = \mathbf{k} - \mathbf{k}_i$ is the wavevector transfer between the incident wavevector $\mathbf{k}_i$ and a general reflected scattering vector $\mathbf{k}$ and f_j is the atomic scattering factor.

We monitored changes in the intensity $I(\mathbf{q}, t) = |A(\mathbf{q}, t)|^2$ from the speckle pattern that results from the (011) Bragg reflection in order to obtain a direct comparison with ultra-fast femto-second coherent X-ray diffraction experiments performed on nanoscale crystals.

Fig. 11 shows the intensity of the resulting speckle patterns' centroid plotted as a function of t. As the total intensity of the speckle pattern is dependent on the amplitude of the complex object, only the relative value of the speckle patterns' intensity is meaningful in the simulations. A characteristic dip lasting for 400 fs is observed immediately before the rutile phase begins at cca. 3.5 ps, which corresponds nicely with the onset of dimerization (Fig. 6). This is also observed experimentally (See Fig. 3 of Newton *et al.*, Ref.[79]) and can be attributed to destructive interference due to disordering at the onset of the structural transition. Rapid spatial variation in V atom sites due to disorder will result in rapid variations in the phase quantity ($\mathbf{q} \cdot \mathbf{u}_j(t)$) in Eq. 4 which when summed, will result in a vanishing scattering intensity.

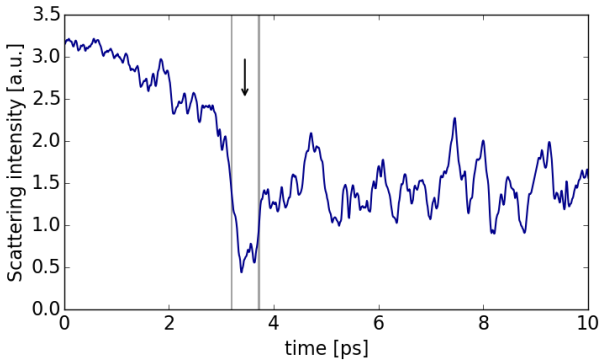

FIG. 11. Scattering intensity of centroid position during simulation at 450 K. A dip in intensity (denoted by arrow) coincides with the onset of the structural transition.

IV. CONCLUSIONS

In summary, we studied the structural and electronic transition in VO_2 by means of *ab initio* molecular dynamics in variable-cell approach, treating both phases on equal footing within a PBE+U description. We show that with suitable choice of the Hubbard U it is possible to observe the temperature-induced transition from M1 to R phase at the transition temperature of 450 K. We found that dimerization and tilting of octahedra evolve at the same time scale and electronic and structural changes occur concurrently, as revealed by detailed microscopic analysis of structural and electronic transformations. The reverse process of dimerization upon cooling the rutile phase was found, however, to be critically contingent upon the rate of cooling. Moreover, we find that the high-temperature rutile phase is characterized by large fluctuations of positions of V atoms, in good agreement with the large value of the Debye-Waller factor known from experiment. We also computed the PDOS for both M1 and R phase and find a good agreement with the experimental data. Our results demonstrate that it is feasible to perform a dynamical study of the structural and electronic transition in VO_2 in fair agreement with experiment, on a system counting several hundreds of atoms. While at the moment the choice of PBE+U functional appears to be the only one, representing a reasonable compromise between computational cost and accuracy, in future it would be certainly interesting to conduct a similar study employing some higher accuracy description of this challenging material. Our simulations also open the way towards simulations of transition in VO_2 induced by photoexcitation, which would be of interest for potential applications to optical switching.

ACKNOWLEDGMENTS

This work was supported by the Slovak Research and Development Agency under Contract APVV-15-0496 and VEGA project No. 1/0904/15 and by the project implementation 26220220004 within the Research & Development Operational Programme funded by the ERDF. This work is funded in part by Royal Society Research Grant

RG/130498. The authors acknowledge the use of the IRIDIS High Performance Computing Facility, and associated support services at the University of Southampton, in the completion of this work. Part of the calculations were also performed in the Computing Centre of the Slovak Academy of Sciences using the supercomputing infrastructure acquired in project ITMS 26230120002 and 26210120002 (Slovak infrastructure for high-performance computing) supported by the Research & Development Operational Programme funded by the ERDF.

* plasienka@fmph.uniba.sk

[1] F. J. Morin, Phys. Rev. Lett. **3**, 34 (1959).
[2] V. Eyert, Ann. Phys. (Leipzig) **11**, 650 (2002).
[3] M. Imada, A. Fujimori, and Y. Tokura, Rev. Mod. Phys. **70**, 1039 (1998).
[4] D. Wegkamp and J. Stähler, Prog. Surf. Sci. **90**, 464 (2015).
[5] K. Okazaki, H. Wadati, A. Fujimori, M. Onoda, Y. Muraoka, and Z. Hiroi, Phys. Rev. B **69**, 165104 (2004).
[6] M. W. Haverkort, Z. Hu, A. Tanaka, W. Reichelt, S. V. Streltsov, M. A. Korotin, V. I. Anisimov, H. H. Hsieh, H.-J. Lin, C. T. Chen, et al., Phys. Rev. Lett. **95**, 196404 (2005).
[7] T. C. Koethe, Z. Hu, M. W. Haverkort, C. Schussler-Langeheine, F. Venturini, N. B. Brookes, O. Tjernberg, W. Reichelt, H. H. Hsieh, H.-J. Lin, et al., Phys. Rev. Lett. **97**, 116402 (2006).
[8] T. Yao, X. Zhang, Z. Sun, S. Liu, Y. Huang, Y. Xie, C. Wu, X. Yuan, W. Zhang, Z. Wu, et al., Phys. Rev. Lett. **105**, 226405 (2010).
[9] J. D. Budai, J. Hong, M. E. Manley, E. D. Specht, C. W. Li, J. Z. Tischler, D. L. Abernathy, A. H. Said, B. M. Leu, L. A. Boatner, et al., Nature **515**, 535 (2014).
[10] J. H. Park, J. M. Coy, T. S. Kasirga, C. Huang, Z. Fei, S. Hunter, and D. H. Cobden, Nature **500**, 431 (2013).
[11] N. B. Aetukuri, A. X. Gray, M. Drouard, M. Cossale, L. Gao, A. H. Reid, R. Kukreja, H. Ohldag, C. A. Jenkins, E. Arenholz, et al., Nat. Phys. **9**, 661 (2013).
[12] A. X. Gray, J. Jeong, N. P. Aetukuri, P. Granitzka, Z. Chen, R. Kukreja, D. Higley, T. Chase, A. H. Reid, H. Ohldag, et al., Phys. Rev. Lett. **116**, 116403 (2016).
[13] Z. Tao, T.-R. T. Han, S. D. Mahanti, P. M. Duxbury, F. Yuan, C.-Y. Ruan, K. Wang, and J. Wu, Phys. Rev. Lett. **109**, 166406 (2012).
[14] A. Pashkin, C. Kübler, H. Ehrke, R. Lopez, A. Halabica, R. F. Haglund, R. Huber, and A. Leitenstorfer, Phys. Rev. B **83**, 195120 (2011).
[15] A. Cavalleri, C. Tóth, C. W. Siders, J. A. Squier, F. Ráksi, P. Forget, and J. C. Kieffer, Phys. Rev. Lett. **87**, 237401 (2001).
[16] A. Cavalleri, T. Dekorsy, H. H. W. Chong, J. C. Kieffer, and R. W. Schoenlein, Phys. Rev. B **70**, 161102(R) (2004).
[17] A. Cavalleri, M. Rini, H. H. W. Chong, S. Fourmaux, T. E. Glover, P. A. Heimann, J. C. Kieffer, and R. W. Schoenlein, Phys. Rev. Lett. **95**, 067405 (2005).
[18] C. Kübler, H. Ehrke, R. Huber, R. Lopez, A. Halabica, J. R. F. Haglund, and A. Leitenstorfer, Phys. Rev. Lett. **99**, 116401 (2007).
[19] P. Baum, D.-S. Yang, and A. H. Zewail, Science **318**, 788 (2007).
[20] M. Hada, K. Okimura, and J. Matsuo, Phys. Rev. B **82**, 153401 (2010).
[21] V. R. Morrison, R. P. Chatelain, K. L. Tiwari, A. Hendaoui, A. Bruhács, M. Chaker, and B. J. Siwick, Science **346**, 445 (2014).
[22] D. Wegkamp, M. Herzog, L. Xian, M. Gatti, P. Cudazzo, C. L. McGahan, R. E. Marvel, J. Richard F. Haglund, A. Rubio, M. Wolf, et al., Phys. Rev. Lett. **113**, 216401 (2014).
[23] H.-T. Kim, Y. W. Lee, B.-J. Kim, B.-G. Chae, S. J. Yun, K.-Y. Kang, K.-J. Han, K.-J. Yee, and Y.-S. Lim, Phys. Rev. Lett. **97**, 266401 (2006).
[24] S. Wall, D. Wegkamp, L. Foglia, K. Appavoo, J. Nag, R. F. H. Jr., J. Stähler, and M. Wolf, Nat. Commun. **3**, 721 (2012).
[25] S. Wall, L. Foglia, D. Wegkamp, K. Appavoo, J. Nag, J. R. F. Haglund, J. Stähler, and M. Wolf, Phys. Rev. Lett. **87**, 115126 (2013).
[26] T. L. Cocker, L. V. Titova, S. Fourmaux, G. Holloway, H.-C. Bandulet, D. Brassard, J.-C. Kieffer, M. A. ElKhakani, and F. A. Hegmann, Phys. Rev. B **85**, 155120 (2012).
[27] R. Yoshida, T. Yamamoto, Y. Ishida, H. Nagao, T. Otsuka, K. Saeki, Y. Muraoka, R. Eguchi, K. Ishizaka, T. Kiss, et al., Phys. Rev. B **89**, 205114 (2014).
[28] V. Eyert, Phys. Rev. Lett. **107**, 016401 (2011).
[29] J. Kim, C. Ko, A. Frenzel, S. Ramanathan, and J. E. Hoffman, Appl. Phys. Lett. **96**, 213106 (2010).
[30] Z. Yang, C. Ko, and S. Ramanathan, Annu. Rev. Mater. Res. **41**, 337 (2011).
[31] G. Stefanovich, A. Pergament, and D. Stefanovich, J. Phys.: Condens. Matter **12**, 8837 (2000).
[32] T. Driscoll, H.-T. Kim, B.-G. Chae, M. D. Ventra, and D. N. Basov, Appl. Phys. Lett. **95**, 043503 (2009).
[33] C. Zhou, D. M. Newns, J. A. Misewich, and P. C. Pattnaik, Appl. Phys. Lett. **70**, 598 (1997).
[34] W.-K. Hong, S. Cha, J. I. Sohn, and J. Kim, J. Nanomater. **2015**, 538954 (2015).
[35] M. A. Kats, R. Blanchard, S. Zhang, P. Genevet, C. Ko, S. Ramanathan, and F. Capasso, Phys. Rev. X **3**, 041004 (2013).
[36] J. B. Goodenough, J. Solid Stat. Chem. **3**, 490 (1971).
[37] A. Zylbersztejn and N. F. Mott, Phys. Rev. B **11**, 4383 (1975).
[38] S. Biermann, A. Poteryaev, A. I. Lichtenstein, and A. Georges, Phys. Rev. Lett. **94**, 026404 (2005).
[39] M. S. Laad, L. Craco, and E. Müller-Hartmann, Phys. Rev. B **73**, 195120 (2006).
[40] Z. Zhu and U. Schwingenschlögl, Phys. Rev. B **86**, 075149 (2012).
[41] M. Gatti, F. Bruneval, V. Olevano, and L. Reining, Phys. Rev. Lett. **99**, 266402 (2007).
[42] J. M. Tomczak, F. Aryasetiawan, and S. Biermann, Phys. Rev. B **78**, 115103 (2008).
[43] R. Sakuma, T. Miyake, and F. Aryasetiawan, Phys. Rev. B **78**, 075106 (2008).
[44] B. Lazarovits, K. Kim, K. Haule, and G. Kotliar, Phys. Rev. B **81**, 115117 (2010).

[45] G.-H. Liu, X.-Y. Deng, and R. Wen, J. Mater. Sci. **45**, 3270 (2010).
[46] R. M. Wentzcovitch, W. W. Schulz, and P. B. Allen, Phys. Rev. Lett. **72**, 3389 (1994).
[47] S. Kim, K. Kim, C.-J. Kang, and B. I. Min, Phys. Rev. B **87**, 195106 (2013).
[48] B. Y. Qu, H. Y. He, and B. C. Pan, J. Appl. Phys. **110**, 113517 (2011).
[49] B. Xiao, J. Sun, A. Ruzsinszky, and J. P. Perdew, Phys. Rev. B **90**, 085134 (2014).
[50] A. Liebsch, H. Ishida, and G. Bihlmayer, Phys. Rev. B **71**, 085109 (2005).
[51] C. Weber, D. D. O'Regan, N. D. M. Hine, M. C. Payne, G. Kotliar, and P. B. Littlewood, Phys. Rev. Lett. **108**, 256402 (2012).
[52] A. S. Belozerov, M. A. Korotin, V. I. Anisimov, and A. I. Poteryaev, Phys. Rev. B **85**, 045109 (2012).
[53] X. Yuan, W. Zhang, and P. Zhang, Phys. Rev. B **88**, 035119 (2013).
[54] H. Zheng and L. K. Wagner, Phys. Rev. Lett. **114**, 176401 (2015).
[55] M. Gatti, F. Sottile, and L. Reining, Phys. Rev. B **91**, 195137 (2015).
[56] W. H. Brito, M. C. O. Aguiar, K. Haule, and G. Kotliar, Phys. Rev. Lett. **117**, 056402 (2016).
[57] S. Kumar, J. P. Strachan, A. L. D. Kilcoyne, T. Tyliszczak, and M. D. Pickett, J. Appl. Phys. **108**, 073102 (2016).
[58] M. A. Korotin, N. A. Shorikov, and V. I. Anisimov, Phys. of Metals and Metallograph. **94**, 17 (2002).
[59] K. Momma and F. Izumi, J. Appl. Cryst. **44**, 1272 (2011).
[60] V. I. Anisimov, J. Zaanen, and O. K. Andersen, Phys. Rev. B **44**, 943 (1991).
[61] A. I. Liechtenstein, V. I. Anisimov, and J. Zaanen, Phys. Rev. B **52**, R5467 (1995).
[62] F. Gervais and W. Kress, Phys. Rev. B **31**, 4809 (1985).
[63] D. B. McWhan, M. Marezio, J. P. Remeika, and P. D. Dernier, Phys. Rev. B **10**, 490 (1974).
[64] G. Kresse and J. Furthmüller, Phys. Rev. B **54**, 11169 (1996).
[65] G. Kresse and J. Furthmüller, Comput. Mat. Sci. **6**, 15 (1996).
[66] G. Kresse and J. Hafner, Phys. Rev. B **47**, 558 (1993).
[67] G. Kresse and D. Joubert, Phys. Rev. B **59**, 1758 (1999).
[68] M. Parrinello and A. Rahman, J. Appl. Phys. **52**, 7182 (1981).
[69] R. Grau-Crespo, H. Wang, and U. Schwingenschlögl, Phys. Rev. B **86**, 081101(R) (2012).
[70] H. Wang, T. A. Mellan, R. Grau-Crespo, and U. Schwingenschlögl, Chem. Phys. Lett. **608**, 126 (2014).
[71] Z. He and A. J. Millis, Phys. Rev. B **93**, 115126 (2016).
[72] S. A. Corr, D. P. Shoemaker, B. C. Melot, and R. Seshadri, Phys. Rev. Lett. **105**, 056404 (2010).
[73] J. M. Longo and P. A. Kierkegaard, Acta Chem. Scand. **24**, 420 (1970).
[74] M. von Laue, Annalen der Physik **26**, 55 (1936).
[75] J. Miao, J. Kirz, and D. Sayre, Acta Crystallographica Section D **56**, 1312 (2000).
[76] M. C. Newton, S. J. Leake, R. Harder, and I. K. Robinson, Nature Materials **9**, 120 (2010), ISSN 1476-1122.
[77] I. Robinson and J. Miao, MRS Bulletin **29**, 177 (2004), ISSN 0883-7694.
[78] I. Robinson and R. Harder, Nature Materials **8**, 291 (2009), ISSN 1476-1122.
[79] M. C. Newton, M. Sao, Y. Fujisawa, R. Onitsuka, T. Kawaguchi, K. Tokuda, T. Sato, T. Togashi, M. Yabashi, T. Ishikawa, et al., Nano lett. **14**, 2413 (2014).